Available online at www.sciencedirect.com
ScienceDirect
International Journal of Heat and Mass Transfer 51 (2008) 3595–3607
International Journal of HEAT and MASS TRANSFER
www.elsevier.com/locate/ijhmt

An experimental and numerical study of stagnation point heat transfer for methane/air laminar flame impinging on a flat surface

Subhash Chander, Anjan Ray *

Department of Mechanical Engineering, Indian Institute of Technology, Delhi, New Delhi 110016, India

Received 29 March 2007; received in revised form 6 August 2007
Available online 26 December 2007

Abstract

A combined experimental and numerical study has been conducted to determine the stagnation point heat transfer for laminar methane/air flame impinging on a flat surface. Effects of Reynolds number, equivalence ratio and burner diameter on stagnation point heat flux were examined experimentally at different separation heights. Maximum stagnation point heat flux was obtained when the flat surface was closest to the tip of the inner premixed reaction zone. Heat flux decreased along the axial direction when the separation distance was further increased from the tip of inner reaction zone. There was a secondary rise in heat flux at the stagnation point at larger separation distances. Correlations were developed for stagnation point Nusselt number. Numerical simulations were carried out using a commercial CFD code (FLUENT) for laminar methane/air flame impinging on a flat surface for various separation distances. Results were compared with those found experimentally. The reason for conducting the simulations was to (a) gain more insight into how the presence of the plate affects the flame and the flow and temperature fields and (b) to explain the reason for high heat flux when the tip of the inner reaction zone was very close to the stagnation point.

Keywords: Premixed flame; Heat flux; Stagnation point; Flat plate; Flame tip

1. Introduction

It is well recognized that metal and glass processing industries require heating of solids of variety of shapes in controlled conditions. In general, rolling and shaping processes for metal and glass are carried out by heating in radiant or electric induction furnaces. The radiant furnaces are believed to have low heating cost but are inefficient and time consuming. The electric induction heating technique is relatively very fast but has problems with respect to adjusting magnetic fields according to shape and size of the job as compared to radiant furnaces. Looking at these difficulties the use of flame impingement heating of solids is becoming attractive even in conventional industries due to the scope of enhanced convective heat transfer rates due to direct contact. This technique has an advantage of increased productivity, reduced fuel consumption and lower pollutant emission from its furnace (Baukal and Gebhart [1]).

Sibulkin [2] investigated the rate of heat transfer at the forward stagnation point for a blunt-nosed body moving through the atmosphere. A semi-analytical relation was given for heat transfer near the forward stagnation point of the body of revolution assuming laminar, incompressible and low speed flow. An important parameter in that relation was the velocity gradient just outside the boundary layer which was a function of nozzle diameter and free stream velocity. Kilham and Purvis [3] studied experimentally the heat transfer to the forward stagnation point of the hemi-spherical nosed probe for premixed methane–oxygen and propane–oxygen flames of various equivalence ratios. Results were compared with those calculated, assuming that (a) recombination reaction of dissociated species are frozen in the boundary layer and the surface is non-catalytic; (b) equilibrium is maintained throughout

* Corresponding author. Tel.: +91 11 26591143; fax: +91 11 26582053.
E-mail address: raya@mech.iitd.ernet.in (A. Ray).

0017-9310/$ - see front matter © 2007 Elsevier Ltd. All rights reserved.
doi:10.1016/j.ijheatmasstransfer.2007.10.018

Nomenclature

A/F	air fuel ratio
C_p	specific heat at constant pressure (kJ/kg K)
d	diameter of the circular nozzle (m)
D	diffusion coefficient
h	enthalpy (kJ/kg)
H	axial distance of the impingement plate from the burner exit plane (m)
H/d	dimensionless separation distance (m/s)
k	thermal conductivity (W/m K)
L_f	flame inner reaction zone length (m)
M	molecular weight (kg/kmol)
Nu	Nusselt number
p	pressure (Pa)
$\dot{q}''$	heat flux (kW/m^2)
r	radial distance (m)
Re	Reynolds number
T	temperature (K)
u	flow velocity (m/s)
υ	flow velocity in x or r direction (m/s)
Y	mass fraction
Z	axial distance between the burner exit plane and the impingement plate measured from stagnation point (m)

Greek symbols

μ	dynamic viscosity (kg-s/m)
ρ	density (kg/m^3)
ϕ	equivalence ratio
δ_f	axial distance between the stagnation point and the tip of the flame inner reaction zone (m)
β	radial velocity gradient in the vicinity of stagnation point

Subscripts

actual	actual state
b	burner rim
exit	at the exit position
i	mixture component including fuel and air
in	inlet mixture
mix	air/fuel mixture
p	plate
r	radial direction
stg	stagnation
stoic	stoichiometric state
x	axial direction

the boundary layer, but the Lewis number of all atoms and radicals is unity; and (c) energy transfer by diffusion and recombination of hydrogen atoms is more rapid than heat transfer by ordinary conduction. These comparisons show that method (a) seriously underestimates the heat transfer and that the experimental values are intermediate between those calculated on the basis of assumption (b) and (c). Conolly and Davies [4] experimentally determined convective heat transfer coefficients at the stagnation point of a blunt body immersed in flames of several common fuel gases burning with pure oxygen. Theoretical predictions of heat transfer were made for the range of conditions studied experimentally. Reasonable agreement between experiment and the numerical semi-empirical predictions was obtained. Fairweather et al. [5,6] presented mathematical models for the prediction of stagnation point heat flux in the chemical equilibrium region of turbulent flames. Experimental measurements of the stagnation point heat flux received by a hemisphere-cylinder probe placed in methane-air flames were included, and free stream temperatures, mean velocities and turbulence intensities were measured for comparisons between theory and experiment. Predictions of the mathematical models show that the influence of free stream turbulence on heat transfer from these flames is relatively small for the considered geometry. Hargrave et al. [7] measured stagnation point heat flux of a body of revolution and a circular cylinder for premixed methane-air flames. Unburnt gas equivalence ratios from 0.8 to 1.2 were examined, with burner exit Reynolds numbers ranging from 2000 to 12,000. Peak heat transfer rates occurred within or close to the flame reaction zone. Van der Meer [8] measured flow structure and heat transfer of impinging flame jets as well as impinging isothermal jets from two rapid-heating burners. The separation distance between burner and plate varied from 1 to 12 burner diameters. The Reynolds numbers of the examined isothermal jets were 3300–10,000. For flame jets, the Reynolds number range was 1700–4250. Stagnation points Nusselt numbers were determined in two ways: from heat flux density measurements and from measurements of the radial velocity gradient in the vicinity of the stagnation point. The results from flame jets agreed quantitatively with the results from isothermal jets if the fluid properties in the heat transfer correlation were taken at a temperature corresponding to the average enthalpy of the boundary layer along the plate.

Many other studies are available (for single flame jet impinging on a flat surface) in the literature (Dong et al. [9–11], Kwok et al. [12], Milson and Chigier [13], Rigby and Webb [14] and Chander and Ray [15]) where the focus was on heat flux measurements in the radial direction. Baukal and Gebhart [1], Viskanta [16,17] and Chander and Ray [18] mentioned in their review papers that flame impingement heat transfer needs further research because of its vast applications in industrial and domestic heating systems. Very recently, Remie et al. [19] have presented analytical relations for calculation of heat flux in the hot spot around the stagnation point for both two-dimensional and axi-symmetric situations of laminar fuel-oxygen flame

impinging on a flat plate. The analysis assumes that a plug flow is generated after the flame front. This assumption, however, is not quite appropriate for fuel-air flame [20].

Kleijn [21] presented a numerical study of heat transfer from laminar, premixed methane/air flames impinging on a flat surface and presented streamlines and isotherms for various cases. He also presented a simple model for stagnation point heat flux in terms of a flame-tip-to-surface distance. However, detailed analysis of how the centerline velocity and temperature as well as the flame length get affected by the plate was not presented. In particular, impinging flames were not compared with a corresponding free flame (i.e., in the absence of a target plate). In the combustion literature, there are studies on a structure of a Bunsen flame (see, for example, Poinsot et al. [22]). However, the influence of an impingement plate on the structure of a Bunsen flame does not seem to be available.

To the authors' knowledge, there is no study in the literature in which the stagnation point heat flux measurements were made at various separation distances for laminar methane/air flame (at low Reynolds number) impinging on a flat surface. In the present study, an experimental investigation has been carried out to measure stagnation point heat flux at various impingement heights for various Reynolds numbers (800–1700), equivalence ratios (0.8–1.2) and for various burner diameters (8–12 mm). As methane is the major constituent of natural gas, the present study will be very useful for understanding the stagnation point heat transfer for many industrial and domestic heating applications. Review of the existing literature also indicated that fundamental understanding of the influence of the plate on the flame and the attendant change in heat transfer characteristics is inadequate. To have a better understanding of stagnation point heat flux variation with separation distance, numerical simulations were carried out using commercially available CFD code FLUENT. Simulations were done for four distinct separation distances, viz., $H/d = 3$, 5, 7 and 9 and also for free flame (without impingement) for $d = 8$ mm, $Re = 1000$ and $\phi = 1.0$. Results were compared with those found experimentally. The influence of the plate on the temperature and velocity fields for various separation distances has been discussed in detail and compared with the situation when there is no target surface (free flame). The results and analysis presented should be of interest from the point of view of heat transfer as well as from a combustion perspective of flame-wall interaction.

2. Experimental facility

Fig. 1 shows the schematic of flame impingement setup. The experimental setup has two major sections; one to facilitate heat generation (burners) and other for heat absorption (calorimeter). Detailed description of the calorimeter and burner assembly was included in our previous published papers [15,23]. Three different burner diameters were used, viz., 8 mm, 9.7 mm and 12 mm to study the effect of burner diameter on stagnation point heat transfer characteristics.

The local heat flux (convective plus radiative) on the impingement surface was measured with a single heat flux micro-sensor (HFM) of 6.35 mm diameter (Vatell Corporation, HFM-7E/H). This heat flux sensor unit also has a provision for surface temperature measurement. High temperature black paint (Zynolite 1000F) covers the sensor surface with spectral emissivity at 2 μm of 0.94. The millivolt (mV) output from the sensor was sensed by a Vatell

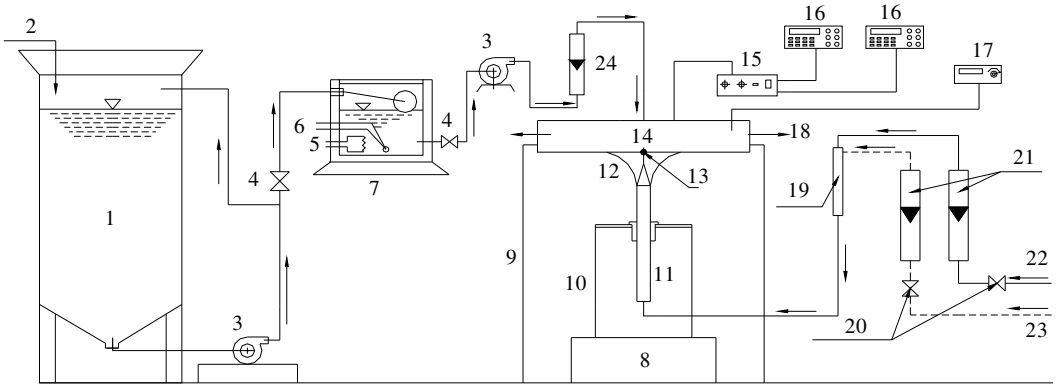

1.Water Tank 2. Inlet Water Supply 3. Pump 4. Flow Control Valve 5. Heating Element 6. Thermostat 7. Insulated Container 8. 3D Positioning Traverse 9. Calorimeter Stand 10. Burner Stand 11. Burner 12. Flame 13. Heat Flux Sensor 14. Calorimeter 15. Signal Conditioning Amplifier 16. Multi-meters 17. Temperature Readout 18. Water Outlet to Waste Tank 19. Mixing Tube 20. Needle Valves 21. Gas Rotameters 22. Air from Cylinder 23. Methane from Cylinder 24. Water Rotameter

Fig. 1. Schematic for single flame jet impingement setup.

Corporation Model AMP-6 signal conditioning amplifier and directed to a Hewlett Packard Model 34401A Multimeter. Based on the calibration of HFM-7E/H sensor the appropriate heat flux was calculated from the output of AMP-6 by the software, *Hfcompv4*, provided by the company. Different commercial rotameters are used for measuring the flow rates of air and fuel respectively. Rotameters are calibrated with DryCal DC-Lite primary gas flow meter. Commercially available methane with 99.99% purity is used and is burnt with synthetic bottled air (Volume %: 21% O_2 and 79% N_2). A 3D mechanism was used for the positioning of the burner.

2.1. Experimental procedure

Measured quantities of air and fuel were mixed in the mixing tube and mixture was fed to the burner. Heated water at a temperature range of 35–45 °C was used as the plate coolant to prevent moisture in the combustion products to condense on the calorimeter surface. Water was supplied to the calorimeter for 15 min before the mixture was ignited to attain temperature uniformity in the experimental setup. All the readings were taken under steady state when the temperature of the outlet water became constant. There was no soot deposition on the surface; still as precaution it was periodically cleaned. First, effect of variation of *Re* on stagnation point heat flux was studied under stoichiometric condition at various separation heights. Starting with *Re* of 800, it was varied up to 1700 for a burner diameter of 9.7 mm. After that, the effect of equivalence ratio was examined at various impingement heights for a fixed *Re* of 1000. Equivalence ratios were varied from 0.8 to 1.2 keeping other parameters constant. Lastly, burner diameter was varied at fixed *Re* and under stoichiometric conditions. The flame jet exit Reynolds number was calculated based on cold fuel/air mixture gases.

$$Re = \frac{u_{\text{exit}} \mathrm{d} \rho_{\text{mix}}}{\mu_{\text{mix}}} \text{ and } \mu_{\text{mix}} = \frac{\sum \left(\mu_i Y_i \sqrt{M_i}\right)}{\sum \left(Y_i \sqrt{M_i}\right)} \tag{1}$$

The equivalence ratio is defined as

$$\phi = \frac{(A/F)_{\text{stoic}}}{(A/F)_{\text{actual}}} \tag{2}$$

3. Uncertainty analysis

Uncertainty analysis was carried out using method given by Kline and McClintock [24]. The uncertainty in the calculated result is estimated based on the uncertainties in the primary measurements. Let result R is a given function of the independent variables $x_1, x_2, x_3, x_4, \ldots, x_n$. Thus,

$$R = R(x_1, x_2, x_3, x_4, \ldots, x_n)$$

If w_R is the uncertainty in the result and $w_1, w_2, w_3, w_4, \ldots, w_n$ are the uncertainties in the independent variables, with the uncertainties in the independent variables of all given with same odds, then the uncertainty in the result having these odds is given as

$$w_R = \left[\left(\frac{\partial R}{\partial x_1} w_1\right)^2 + \left(\frac{\partial R}{\partial x_2} w_2\right)^2 + \left(\frac{\partial R}{\partial x_3} w_3\right)^2 + \ldots\ldots + \left(\frac{\partial R}{\partial x_n} w_n\right)^2 \right]$$

Uncertainties in equivalence ratio and Reynolds number were 2.83% and 2.2% respectively. Maximum uncertainty in heat flux measurements was 5.88%.

4. Results and discussion

4.1. Experimental results

4.1.1. Effect of Re

Fig. 2 shows the stagnation point heat flux profiles for a methane/air flame impinging on a flat surface for various Reynolds numbers under stoichiometric condition. The axial distance on the abscissa indicates the distance measured along the burner axis from the burner exit plane to the target surface. For a small axial separation distance (H), the inner reaction zone was intercepted by the plate and the stagnation point heat flux was zero or even negative. This was because of direct impingement of cool un-burnt mixture on the impingement surface [13,15,23,25].

On increasing H, it was found that the heat flux was very low till the tip of the inner reaction zone started touching the impingement surface. As the tip of the inner reaction zone touched the impingement surface, a sudden rise in heat flux was obtained with heat flux attaining the peak value. This magnitude of peak heat flux increased with increase in the value of *Re*. The axial distance corresponding to the peak heat flux also increased with increase with *Re*. The magnitudes of peak stagnation point heat fluxes were 385 kW/m^2, 420 kW/m^2, 460 kW/m^2 and 521 kW/m^2 at axial locations of 19 mm, 22.5 mm, 27.5 mm and 38 mm for *Re* of 800, 1000, 1300 and 1700 respectively.

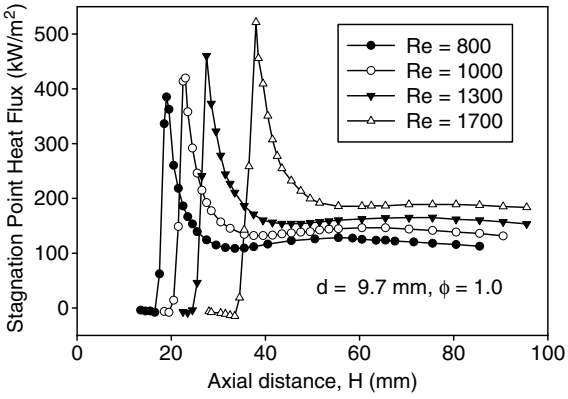

Fig. 2. Stagnation point heat flux profiles for various values of Reynolds number at different axial locations for $d = 9.7$ mm and $\phi = 1.0$.

The results of numerical simulation presented in this article provide greater clarity on the issue of peak heat flux.

Axial length corresponding to which peak heat flux occurs indirectly represents the length of the flame inner reaction zone. As the separation distance was increased beyond the tip of the inner reaction zone, for all *Re*, stagnation point heat flux decreased and reached a local minimum corresponding to certain value of axial distance. This distance was different for different *Re*. At these points, the flame gases are assumed to be approximately in chemical equilibrium [7]. With further increase in separation distance, higher than these minimum heat flux points, the stagnation point heat flux showed an increase up to some separation height. Beyond this height, the heat flux monotonically decreased. This secondary maximum in heat flux was more prominent for lower *Re*.

4.1.2. Effect of equivalence ratio

Fig. 3 shows the stagnation point heat flux profiles at various equivalence ratios at $Re = 1000$. Flames were longer for leaner and richer mixtures compared to near-stoichiometric condition. This was because of lesser value of burning velocity for leaner and richer mixtures. The flame was longest for $\phi = 1.2$. For $\phi = 1.2$, the measured peak heat flux was lower at the stagnation point compared to $\phi = 0.8$ or $\phi = 1.0$. The peak stagnation point heat flux values were 388 kW/m^2, 420 kW/m^2 and 364 kW/m^2 at axial locations of 24.5 mm, 22.5 mm and 32.5 mm for $\phi =$ 0.8, 1.0 and 1.2 respectively. There was a slight secondary rise in heat flux up to some axial distance for all the equivalence ratios examined.

4.1.3. Effect of burner diameter

Fig. 4 shows the comparison of stagnation point heat flux for different burner diameters under identical operating conditions for various impingement heights for $Re = 1000$, $\phi = 1.0$. Similar to the previous cases, the peak heat flux occurred at the separation distance when the tip of the inner reaction zone was just touching the target surface. As the value of *Re* was the same, in all the cases the peak heat flux occurred at the same separation distance from the exit plane of the burner (~23 mm). Peak heat fluxes of 473 kW/m^2, 420 kW/m^2 and 375 kW/m^2 were obtained for burner diameters of 8, 9.7 and 12 mm respectively. Thus, the maximum heat flux was recorded corresponding to minimum burner diameter. This was because for same *Re* the minimum diameter would produce the highest value of axial velocity, hence the highest value of axial velocity gradient, resulting in the highest convective heat transfer. After crossing the peak at the tip of the flame, heat flux decreased to some local minimum before increasing further at some higher separation distance. Secondary increase in heat flux was more significant for larger burner diameters for same value of *Re*. For 8 mm burner diameter, this increase was not so significant. After crossing the secondary peak in heat flux, the heat flux monotonically decreased with increase in separation distance.

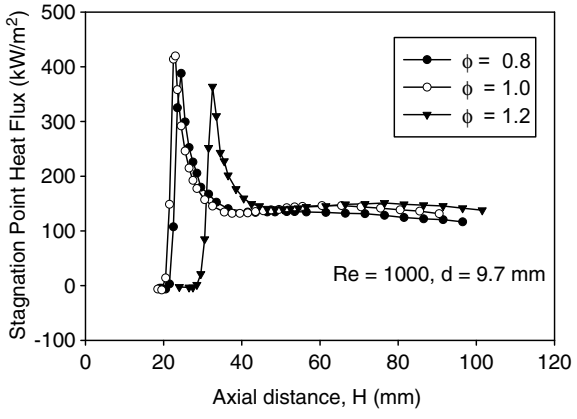

Fig. 3. Stagnation point heat flux profiles for various values of equivalence ratio at different axial locations for $d = 9.7$ mm and $Re = 1000$.

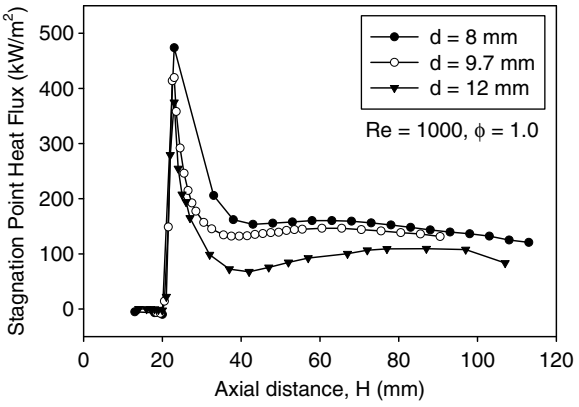

Fig. 4. Stagnation point heat flux at various separation distances for different burner diameters under identical operating conditions of $Re = 1000$ and $\phi = 1.0$.

4.2. Stagnation point Nusselt number correlations

Stagnation point Nusselt number correlations have been developed in terms of *Re* and δ_f for $\phi = 1.0$. Fig. 5 illustrates the problem configuration and indicates the dimension δ_f. Kleijn [21] showed that the stagnation point heat flux $\propto \delta_f^{-1/2}$. For the experimental data of the present

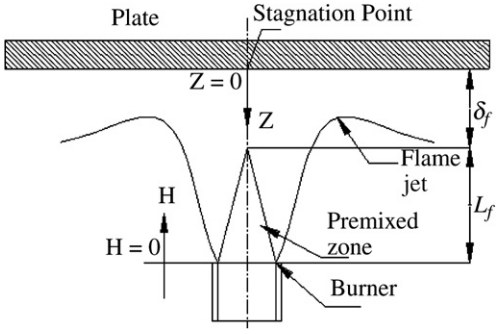

Fig. 5. Impinging flame shape.

study, stagnation point heat flux was plotted against $\delta_f^{-1/2}$ (Fig. 6). Stagnation point heat flux was proportional to $\delta_f^{-1/2}$ along the axial length from the tip of the inner reaction zone up to the start of the secondary rise in heat flux. Stagnation point Nusselt number is defined by Eq. 3;

$$Nu_{stg} = \frac{\dot{q}''_{stg} \times d}{k \times (T_{f,stg} - T_{p,stg})} \tag{3}$$

where T_f is the flame temperature (here it is taken as the adiabatic flame temperature (2235 K)) and $T_{p,stg}$ is the plate temperature at the stagnation point. Here, k is the thermal conductivity (W/mK) of the combustion products, evaluated at $0.5(T_f + T_{p,stg})$ and d is the burner diameter in meters.

A dimensionless correlation (as given in Eq. 4) for stagnation point Nusselt number (valid for $H > L_f$) was developed for stoichiometric condition:

$$Nu_{stg} = 13\left(\frac{\delta_f}{L_f}\right)^{-0.2397}\left(1 - \frac{410}{Re}\right) \text{ with } R^2 = 0.9013 \tag{4}$$

Maximum over-prediction of experimental data was by 29% and under-prediction by 36%. These large errors were due to secondary increase in heat flux after crossing the tip of the flame along the burner axis. Another correlation (Eq. 5) was developed for the stagnation point Nusselt number from tip of the flame up to start of secondary increase in heat flux (excluding far-off points). For this correlation, the maximum over-prediction reduced to 6% and under-prediction to 6.5%.

$$Nu_{stg} = 7.3\left(\frac{\delta_f}{L_f}\right)^{-0.357}\left(1 - \frac{300}{Re}\right) \text{ with } R^2 = 0.9912 \tag{5}$$

L_f can be calculated with the approximate relation given by Kleijn [21]:

$$\frac{L_f}{d} = \frac{v_{in}}{2v_f} \tag{6}$$

Here, v_{in} was the average inlet velocity of the mixture coming out from the tube and v_f was the burning velocity.

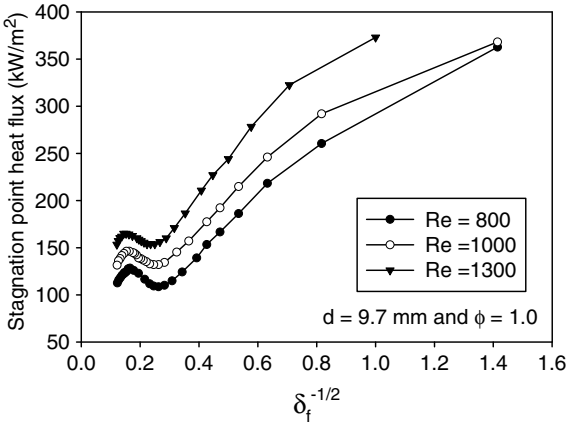

Fig. 6. Stagnation point heat flux vs. $\delta_f^{-1/2}$ for $d = 9.7$ mm, $\phi = 1.0$ for different Reynolds numbers.

The above equation is obtained by assuming the reaction zone to be a perfect right circular cone whose surface area can be approximated as $\frac{1}{2}\pi d L_f$, since $v_{in} \gg v_f$ in our case.

So, for a given H, δ_f will equal $(H - L_f)$. Curve-fit for the correlation (Eq. 5) with experimental data is shown in Fig. 7. The correlation showed good agreement except near the tip of the inner reaction zone.

4.3. Numerical simulation

In the present study, FLUENT [26] (commercial CFD software) was used to model the flow field and heat transfer for premixed laminar methane/air flame impinging on a flat surface with a reduced (same as that of Kleijn [21]) reaction mechanism (16 species and 25 reactions). The results obtained from the simulation were verified the experimental results. The general form of transport equation for two dimensional transient axi-symmetric laminar reactive flow can be written as:

$$\frac{\partial}{\partial t}(\rho\phi) + \frac{\partial}{\partial x}(\rho v_x \phi) + \frac{1}{r}\frac{\partial}{\partial r}(r\rho v_r \phi) = \frac{\partial}{\partial x}\left(\Gamma\frac{\partial \phi}{\partial x}\right) + \frac{1}{r}\frac{\partial}{\partial r}\left(r\Gamma\frac{\partial \phi}{\partial r}\right) + S_\phi \tag{7}$$

where ϕ denotes $1, v_x, v_r, h, Y_i$ and general diffusion coefficient Γ is $0, \mu, \mu, \frac{k}{C_p}$ and D_{im}respectively. S_ϕ is a source term. FLUENT uses a control-volume-based technique to convert the governing equations to algebraic equations that can be solved numerically.

4.3.1. Computational domain

The modeling of the problem was done in Gambit 2.0 (Fluent Inc.), a preprocessor for Fluent 6.1, and the schematic of this model along with the various boundary conditions are shown in Fig. 8.

Using the axi-symmetric condition, 2D model has been used. In the model, the impingement surface reduces to a

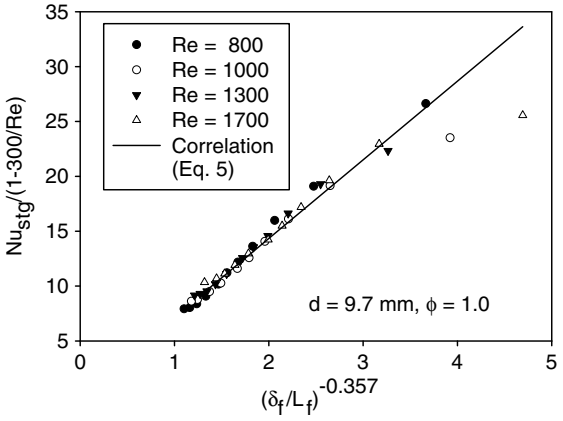

Fig. 7. Curve-fit for stagnation point Nusselt number correlation (starting with tip of the flame up to the start of the secondary rise in heat flux) for various values of Reynolds numbers at different axial locations for $d = 9.7$ mm and $\phi = 1.0$.

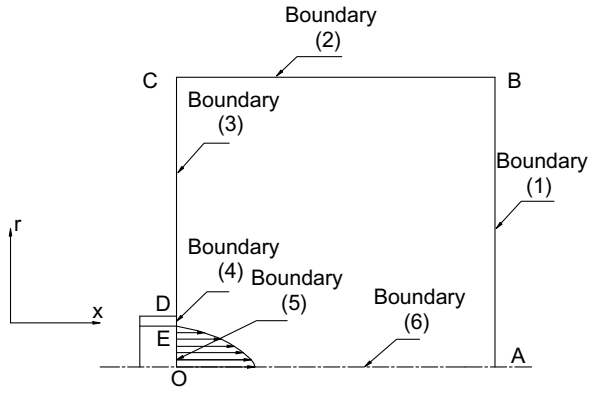

Fig. 8. Schematic of model taken in the simulation for flame impingement.

line AB, half of the burner exit is represented by EO, which is also the burner tube radius. DE is the tube-wall, and OA is the tube axis. BC and CD are the boundaries of the model, which bound the flow, and hence limit the computational flow domain.

4.3.2. Boundary conditions

Different boundary conditions were discussed below:

I. *Impingement surface (boundary (1))*: The impingement surface has been treated as a wall, i.e. no-slip boundary condition was applied, and therefore all the velocity components were zero at this boundary. So boundary conditions at boundary (1) were

$$v_x = 0 = v_r \text{ and } T_p = 300 \text{ K}$$

It has to be noted here that the plate temperature was not fixed at 300 K in the experiments and it has a variation in the radial direction. However, moderate variations in plate temperature did not affect the simulation results significantly. Hence, an imposed plate temperature of 300 K was considered to be adequately accurate for our purpose.

II. *Boundary (2)*: As r tends to infinity, the total flow pressure will become atmospheric, and all the velocity components will tend to zero. These constraints have been achieved by treating this boundary as pressure-outlet (i.e. flow moving out from the boundary at some pressure p) and the total gauge pressure is given as zero. So boundary condition at boundary (2) was

$$p = p_{atm}$$

Ideally boundary (2) must be placed at infinity from the axis of the flow so that the total pressure becomes atmospheric. In the simulations, a sufficiently large domain was chosen to meet the above conditions.

III. *Boundary (3)*: The constraints to be imposed at this boundary are same as that of boundary (2), with the only difference that it has been treated as pressure-inlet (flow moving into the domain with some pressure p). Thus, at this boundary;

$$p = p_{atm}, v_x = 0, v_r = 0, T = 300 \text{ K and } Y_{O_2} = 0.23$$

IV. *Boundary (4)*: This boundary was burner rim and was kept at constant temperature (300 K), so at this boundary, $T_b = 300$ K, $v_x = 0$ and $v_r = 0$.

V. *Boundary (5)*: A fully developed parabolic exit-velocity profile was assumed in the analysis, and therefore the axial velocity at the exit of the nozzle has a parabolic variation with the radius (boundary (5)). The velocity in the radial direction was zero at this boundary i.e., $v_x = f(r)$, $v_r = 0$ and $T_{in} = 300$ K.

Here, $v_x = (f(r))$

$$= (v_x)_{max}\left[1 - \left(\frac{r}{R}\right)^2\right] \text{and also } (v_x)_{max} = 2\bar{v}_x$$

$(v_x)_{max}$ and $\bar{v}_x$ were maximum and average axial velocities and R was radius of burner tube. Also, the mass fractions of different species in the incoming mixture were:

$$Y_{CH_4} = 0.055, Y_{O_2} = 0.22, Y_{N_2} = 0.725$$
$$\text{for air}(21\%\ O_2; 79\%\ N_2)$$

VI. *Boundary (6)*: This boundary represents the centerline of the burner or axis of symmetry. Here, the boundary conditions were

$$v_r = 0 \text{ and } \frac{\partial()}{\partial r} = 0$$

VII. In case of free flame simulation, boundary (1) was treated as pressure-outlet (same as II) and boundaries (2) and (3) were treated as pressure-inlet (as discussed in III).

4.3.3. Computational grid

Computational grids were made in Gambit 2.0 (Fluent Inc.). An inner burner diameter of 8 mm was used for all simulation cases. A very fine grid was used in the flame region and also in the region near the impingement surface. Similar to the work of Kleijn [21], a non-uniform grid was used with grid cell dimensions $\Delta r = 50$ μm and $\Delta x = 200$ μm in the flame region. Grid independency check was done by considering the finest grid. Heat flux was predicted within 1.5% of the values obtained on the finest grid ($\Delta r = 25$ μm and $\Delta x = 100$ μm).

For all H/d, within the flame zone (i.e., $0 \leqslant r \leqslant 5$ mm and $0 \leqslant x \leqslant 25$ mm), the grid consisted of uniform grid cells with dimensions $\Delta r \times \Delta x$. Near the impingement surface (i.e., $0 \leqslant Z \leqslant 5$ mm), the axial dimension of the grid cell was smoothly decreased from Δx to $0.25\Delta x$ in order to accurately resolve the thermal boundary layer. For $r > 5$ mm, the radial dimension of grid cells was smoothly increased from Δr to $30\Delta r$.

4.3.4. Computational technique

FLUENT 6.1 was employed to simulate mass, momentum, and heat transfer by solving a set of non-linear governing equations in each cell. The steady mode was chosen. The second order upwind scheme was used for the discretization of non-linear equations. The double-precision segregated solver was utilized with implicit method of advancing toward the solution. A laminar combustion species transport model was used with finite rate chemistry. Arrhenius rate equation was used to determine the rate of the formation of species. The methane/air combustion mechanism is very complex and consists of hundreds of elementary reactions between dozens of intermediate gas species. A reduced (same as that of Kleijn [21]) chemical reaction mechanism (25 reactions and 16 species) was imported in CHEMKIN format along with thermodynamic database. Multiple simultaneous chemical reactions were modeled with reactions occurring in the bulk phase (volumetric reactions).

4.3.5. Thermo-chemical properties input

Thermo-chemical properties of the gas species as a function of temperature have been taken from CHEMKIN thermo-dynamical database. Temperature and species dependence was imposed in calculations of thermodynamic and transport properties. Viscosity of the individual species was calculated by using kinetic theory. The mixture viscosity was calculated using ideal gas mixing law. Thermal conductivity for individual species was calculated using kinetic theory. Specific heat capacity of individual species was calculated using piece-wise-polynomial approximation. Here, the Maxwell–Stefan equations were used to obtain the diffusive mass flux.

4.3.6. Computational procedure

Methane/air flame impingement model for solution by FLUENT was set up for a 2D axi-symmetric computational domain using segregated solver. The initial guesses for velocity, temperature and mass fraction of oxygen and methane were set to constant values over the entire computational domain. Once the boundary conditions were set, the flow field for non-reacting case was calculated, with all species conservation equations and momentum equation active. An under-relaxation factor of 0.1 was given to all species equations and 0.05 to energy equation. Energy equation and volumetric reactions were kept off during cold flow solution calculations. The solution was run for 1500–2000 iterations till the residuals for radial and axial velocities got settled. Then the mixture was ignited. To ignite the mixture a region of cells above the burner exit was artificially assigned a temperature of 1700 K. Now, the energy equation and volumetric reaction were activated and reaction source term relaxation factor was set to 0.1. Sometimes, it was observed that ignition did not take place in the first run. In such cases, after running the solution for a few iterations, the solution was interrupted. Cells with temperature range of 500–1200 K were again set to high temperature, may be 1900 K or 2000 K. This procedure was repeated till the ignition actually started. Once the ignition took place, the under relaxation factor for all species equation and energy equation was set to 0.5 and 0.3 respectively. The reaction source term relaxation factor was increased to 0.8. Solution converged in about 17,000 to 20,000 iterations after the relaxation factors had been increased. For convergence, residual for methane species equation should be less than 1×10^{-05}. The continuity equation residual should be less than 1×10^{-08}.

4.3.7. Numerical results

Numerical simulation using commercial CFD software (FLUENT) was carried out for 8 mm-diameter burner. The plate temperature was 300 K. The mixture flow was with $Re = 1000$ and mixture was stoichiometric. The air composition was the same as that of experimental conditions, i.e., volume %: 21% O_2 and 79% N_2. To investigate the effect of separation distance on stagnation point heat flux, simulations were carried out for four distinct separation distances, viz., $H/d = 3$, 5, 7 and 9. Simulations were also done for free flame (under identical operating conditions) to compare with impingement situations to understand the effect of the presence of impingement plate on the flame and on the velocity and temperature fields.

4.3.7.1. Simulated and experimental stagnation point heat fluxes. Fig. 9 shows the comparison of stagnation point heat flux at various separation distances (H/d) obtained both by simulation and experiments. The H values considered in this plot were all greater than the flame length, i.e., L_f. Simulation results under-predicted the experimental results for all H/d. The difference in results between experiments and simulation can be due to several factors. The prime reason, however, was because of slightly shorter flame lengths predicted by simulation in comparison to experiments. Shorter flame lengths in simulation were possibly because of the use of reduced reaction mechanism resulting in overestimation of burning velocity. Thus, for

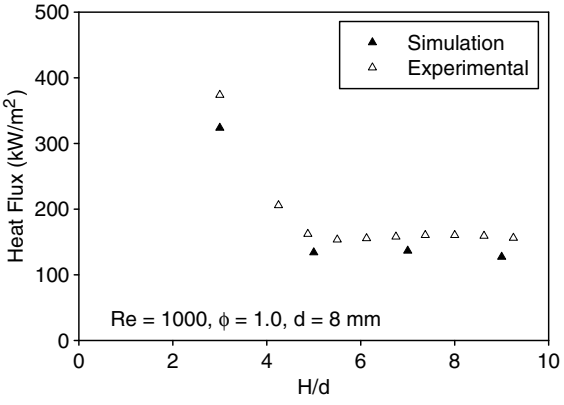

Fig. 9. Comparison of experimental and simulation results for stagnation point heat flux at various separation distances.

a fixed value of H/d, the tip of the inner reaction zone was at a slightly larger distance from the stagnation point in simulation compared to the corresponding value in experiments. The proximity of the flame inner reaction zone to the surface significantly affects the heat flux value at the stagnation point (Chander and Ray [15]). Additionally, radiation model was not used in the present simulation. Even for non-luminous flames, the radiation component can be up to 5% (Hoogendoorn et al. [27]) of the total heat transfer to the surface. Inclusion of radiation model in simulation would have increased the computation time many-folds. Already, one simulation case was taking around 17000–20000 iterations for complete convergence. The total time taken on 2.8 GHz, 256 Mb RAM machine was more than five days. Finally, there were experimental uncertainties also, as indicated in Section 3, contributing to the differences between the experimental and simulated values.

The peak in the heat flux profile occurred at $H/d = 3$ (the case when the tip of the inner reaction zone was close to the impingement surface). After crossing the peak in heat flux near the tip of the inner reaction zone there was a drop in the values obtained both in experiments and simulation. Further along the axis at large separation distances the heat flux increased to slightly higher values and reached a secondary maximum. Thereafter, the stagnation point heat flux decreased from $H/d = 7$ to $H/d = 9$ at a slow rate. As mentioned earlier (Fig. 4), the secondary rise in heat flux for smaller burner diameters was not appreciable compared to larger burner diameters. For 8-mm diameter burner the heat flux remained almost constant from $H/d = 5$ to $H/d = 9$.

4.3.7.2. Velocity, temperature and pressure profiles. Fig. 10 shows the simulated variation of centerline velocity and temperature for methane/air free flame (not impinging) at $Re = 1000$ and $\phi = 1.0$. Centerline velocity remained almost constant till the tip of the inner reaction zone ($H \sim 22$ mm). A slight dip in the velocity occurred just before attaining the peak at the tip of the inner reaction zone. This dip in velocity value before the start of the inner reaction zone was due to divergence of the central stream tube as it passed through the preheat zone causing the velocity of flow to lower until it matched with the burning velocity locally at the start of the reaction zone (Strehlow [28]).

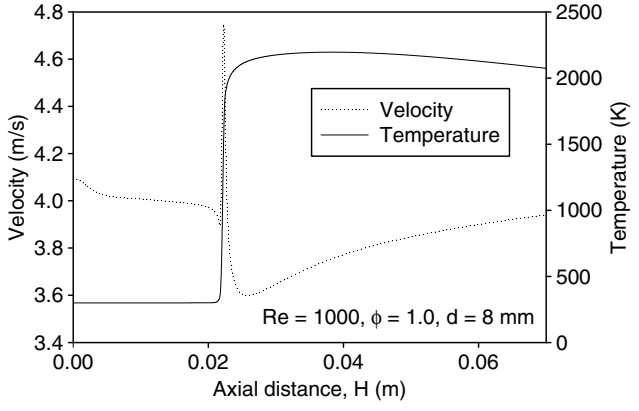

Fig. 10. Simulated centerline velocity and temperature variation for free flame.

The centerline velocity profile exhibited a peak at the tip of the flame, i.e., at the location where the temperature underwent a sudden increase. This peak in the centerline velocity at the tip was due to the high temperature of the combustion products in that region resulting in decreased density and increased axial velocity.

Immediately after crossing the peak there was a sudden fall in velocity because of flow divergence at the tip of the flame away from axial direction. Further in the downstream direction, the gradual increase in axial velocity can be attributed to the convergence of streamlines in the downstream direction (as shown in Fig. 11). Just ahead of the tip of the inner reaction zone, centerline temperature was same as that of the unburnt mixture. Right at the tip, there was a sudden jump in the temperature due to combustion heat release. Even beyond the tip of the inner reaction zone, centerline temperature still increased because of burning of H_2 and CO in the outer diffusion flame zone. Peak temperature of nearly 2235 K was obtained which was very close to the adiabatic temperature for stoichiometric mixture of methane/air.

Fig. 12 shows the pressure (gauge) contours for free flame around the tip region. A slight variation in pressure was noticed at and around the reaction zone at the tip. The pressure just before the tip was a little higher resulting in the dip in the centerline velocity value before the reaction zone (as shown in Fig. 10). At the tip of the reaction zone and also just beyond that, pressure was lower, accompanied by an increase in centerline velocity. Further downstream, the pressure was low but kept increasing with axial distance till it matched with the local atmospheric pressure. All along the reaction zone pressure was sub-atmospheric.

Figs. 13 and 14 show the comparison of axial velocity for free and impinging flames for two distinct cases. Fig. 13 shows the comparison of centerline velocity for $H/d = 9$. Centerline velocity profiles for free and impinging flames were exactly the same up to the tip of the inner reaction zone indicating that the effect of the presence of impingement plate on inner reaction zone was insignificant. After the sudden jump in the velocity at the tip of the flame, the axial velocity, in case of the free flame, decreased followed by gradual increase in the downstream direction. For the impingement case ($H/d = 9$), the presence of the plate was felt immediately after the dip in velocity. The axial velocity started deviating from the free flame centerline velocity profile and decreased at a high rate some distance away from the tip after an initial increase. The axial velocity then decreases to zero at the stagnation point.

Fig. 14 shows the comparison of centerline velocity profile with ($H/d = 3$) and without impingement plate. Compared to the previous case (for $H/d = 9$), the effect of the

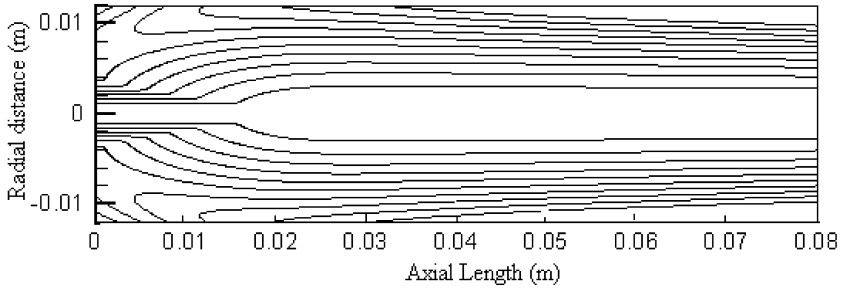

Fig. 11. Stream function profiles for free flame ($Re = 1000$, $\phi = 1.0$, $d = 8$ mm).

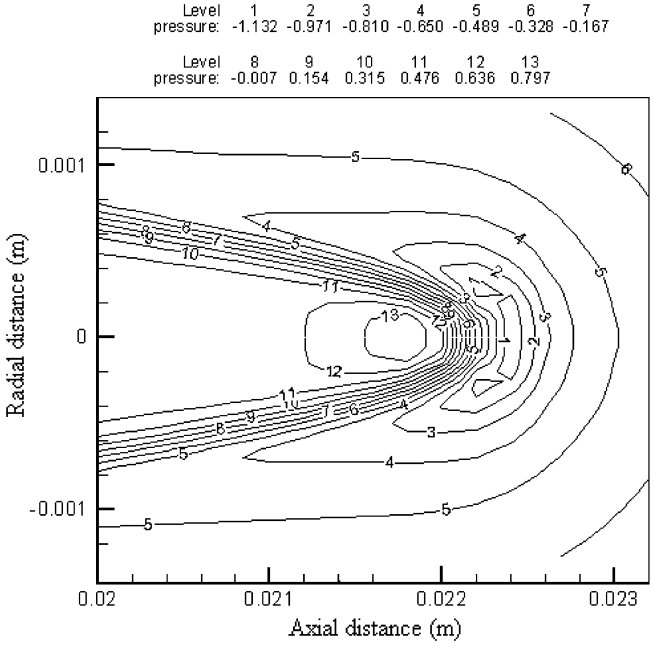

Fig. 12. Static pressure (gauge pressure in Pascal) for free flame near the tip ($Re = 1000$, $\phi = 1.0$ and $d = 8$ mm).

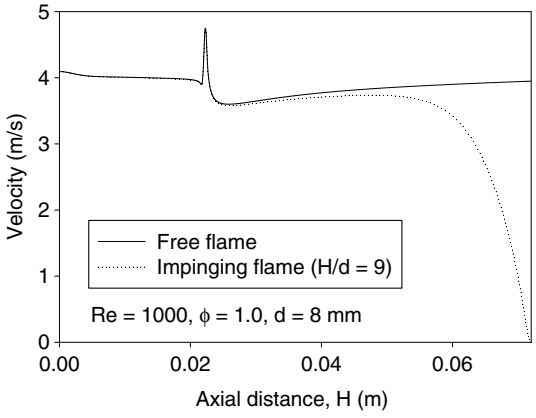

Fig. 13. Comparison of simulated centerline velocity for free flame and impinging flame for $H/d = 9$.

presence of the plate was more significant. The jump in the centerline velocity at the tip of the reaction zone was at shorter axial length in the presence of the plate compared

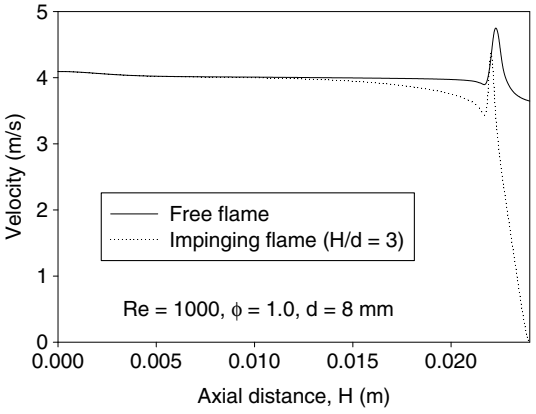

Fig. 14. Comparison of simulated centerline velocity for free flame and impinging flame for $H/d = 3$.

to the free flame. This indicated a shift in the flame reaction zone towards the exit plane of the burner, i.e., a shorter flame length because of the presence of the plate. The axial velocity profile was also affected in the unburnt gas region inside the reaction zone.

Figs. 15a and 15b show the simulated profiles for axial temperature and velocity for $H/d = 3$ and $H/d = 5$ respectively. All other operating conditions were kept constant ($Re = 1000$ and $\phi = 1.0$). These two separation distances represented two distinct cases, viz., tip of the inner reaction zone close to the impingement surface and away from the

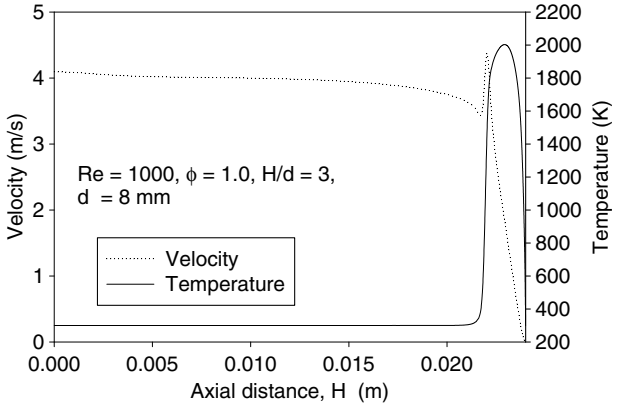

Fig. 15a. Simulated centerline velocity and temperature profiles for $H/d = 3$ ($Re = 1000$, $\phi = 1.0$ and $d = 8$ mm).

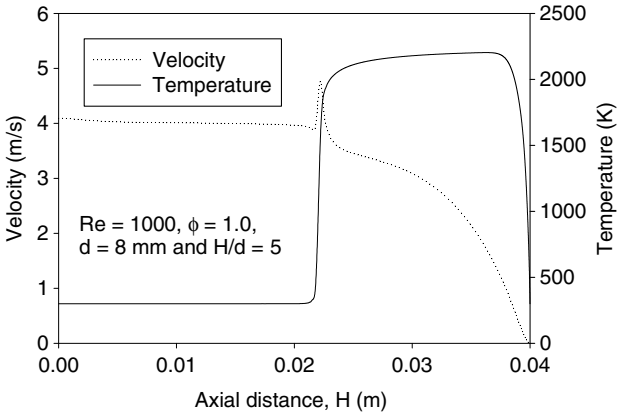

Fig. 15b. Simulated centerline velocity and temperature profiles for $H/d = 5$ ($Re = 1000$, $\phi = 1.0$ and $d = 8$ mm).

impingement surface. Figs. 15a and 15b indicate that there were sudden rises in the axial velocity and temperature distributions at the tip of the flame inner reaction zone. Centerline peak temperature decreased when the location of the flame tip was closer to the impingement surface (lower for $H/d = 3$ compared to $H/d = 5$). This was because of greater heat loss to the surface from the flame tip when it was closer to the impingement surface. Also, the temperature gradient was steeper when the flame tip was closer to the surface. This affected the heat flux at the stagnation point, as heat transfer to the surface is directly proportional to temperature gradient. The centerline temperature decreased to the specified value of 300 K at the impingement surface.

Fig. 16 shows the variation of axial velocity near the stagnation point for different separation distances. In all cases, at the tip of the inner reaction zone, there was sudden increase in the axial velocity. When the inner reaction zone was closest to the impingement surface ($H/d = 3$), the velocity gradient at the stagnation point was very high. For larger separation distances ($H/d = 5$, 7 and 9), when the tip of the inner reaction zone was away from the impingement surface, the velocity gradient was quite low compared to

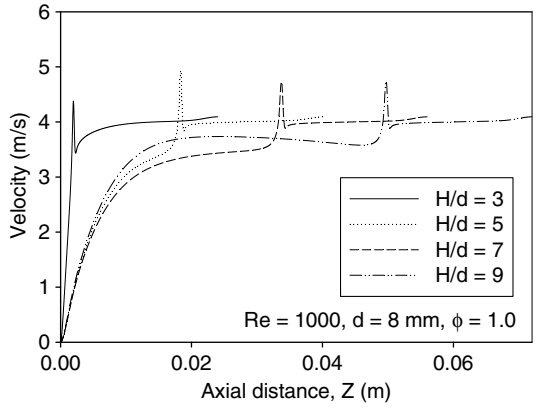

Fig. 16. Simulated centerline velocity variation near the stagnation point for different separation distances under identical operating conditions.

$H/d = 3$. Interestingly, the velocity gradient at the stagnation point in the axial direction for $H/d = 9$ was greater than those for $H/d = 5$ and 7. This was because of lesser influence of the presence of plate near the tip of the inner reaction zone for $H/d = 9$. For $H/d = 9$, the combustion products had sufficient length to get accelerated after the initial dip in velocity just after the tip of the inner reaction zone prior to the deceleration caused by the plate (Fig. 13). On the other hand, for $H/d = 5$ and 7, axial velocity monotonically decreased beyond the flame tip since the retarding influence of the plate did not allow the secondary increase in flow velocity away from the tip of the reaction zone.

Fig. 17a and b shows the axial temperature variation at different separation distances. Fig. 17b shows the magnified view of the temperature profiles near the stagnation point. The temperature gradient at the impingement surface was very sharp for $H/d = 3$. For other separation distances, $H/d = 5$, 7 and 9, the temperature gradients near the surface were not very different from one another. High heat flux at the stagnation point when the tip of the inner reaction zone just touched the impingement surface (i.e. for $H/d = 3$) can be attributed to this large value of the temperature gradient near the surface. Heat fluxes at $H/d = 5$, 7 and 9 were considerably less (Fig. 9) compared to at $H/d = 3$ because of lesser temperature gradient in the axial

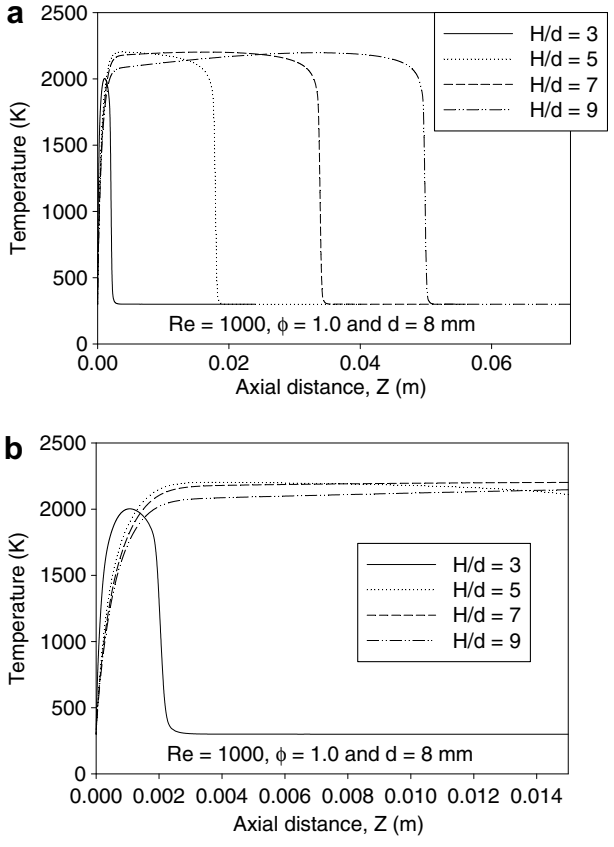

Fig. 17. Simulated centerline temperature variation near the stagnation point for different separation distances under identical operating conditions.

direction. It has to be mentioned, however, that close to the high temperature zone, large concentration of reactive species such as atoms and free radicals exists which augment convective heat transfer rates by diffusion and exothermic recombination in the boundary layer surrounding the target surface [7]. This effect was not taken into account in the present simulations of methane/air flames. This effect is expected to be pronounced for oxy-flames and is not considered to be very significant when the oxidizer used is air [29].

In summary, the velocity and axial temperature gradients were highest for $H/d = 3$ and consequently the stagnation point heat flux. For $H/d = 5$, 7, and 9, the centerline velocity and temperature gradients at the plate were all comparable. Thus, the stagnation point heat flux values were almost the same for these three H/d values. Interestingly, the centerline velocity gradient is higher for $H/d = 9$ compared to $H/d = 5$ and 7. In contrast, the temperature gradient for $H/d = 9$ was lower compared to $H/d = 5$ and 7.

The simulation results indicate that the secondary peak in heat flux profile (see Fig. 4, for example) is probably due to the following reason. Immediately above the flame tip, there is a drop in axial velocity, leading to a minimum in heat flux. However, Fig. 16 shows that further away from the tip, the centerline axial velocity increases with distance, providing for a higher velocity gradient at the plate. This effect can increase the heat flux at the plate. On increasing the separation distance further, the effect of increase in axial velocity gradient is offset by a decrease in the temperature of the combustion gases approaching the plate due to entrainment of ambient air and the heat flux starts reducing from the value attained at the secondary peak. Fig. 17 illustrates the drop in temperature for higher values of $H/d = 9$. The secondary peak, however, was almost insignificant in the simulation results for the 8-mm-diameter burner.

4.3.7.3. Radial velocity profiles. Fig. 18 shows the radial velocity profiles for different separation distances along a line parallel to the plate surface at close vicinity of the stagnation point ($Z = 0.1$ mm).

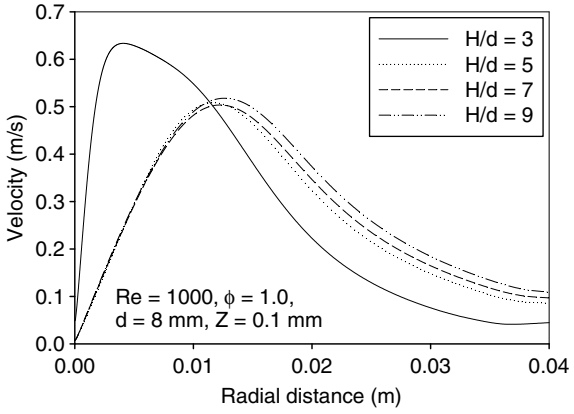

Fig. 18. Simulated radial velocity variations for different separation distances under identical operating conditions for $Z = 0.1$ mm.

The velocity increased in the radial direction because of favorable pressure gradient, till it attained peak at some radial location. After that the radial velocity decreased further in the wall-jet region. The magnitude of velocity peak was largest for $H/d = 3$. In the wall-jet region the velocity profile trends reversed with high velocity for $H/d = 9$ and least velocity for $H/d = 3$. Largest velocity gradient was observed near stagnation point for $H/d = 3$. Velocity gradient for other separation distances ($H/d = 5$, 7 and 9) were small compared to $H/d = 3$. Sibulkin [2] developed a semi-analytical relation for stagnation point heat transfer of a body of revolution in uniform cross flow. Stagnation point Nusselt number was related to a parameter β (radial velocity gradient in the vicinity of the stagnation point). Van der Meer [8] reported that the velocity gradient in the vicinity of stagnation point (β) strongly influenced the stagnation point heat transfer for low Reynolds number turbulent flame jets impinging on a flat surface. Fig. 18 confirms that the radial velocity gradient in the vicinity of the stagnation point is very important in determining the magnitude of the stagnation point heat flux.

5. Conclusions

A combined experimental and numerical study has been carried out to investigate stagnation point heat flux for laminar methane/air premixed flame impinging on a flat surface and to investigate the influence of the plate on the flame and the axial velocity and temperature profiles. Following conclusions were arrived at:

1. Stagnation point heat flux for laminar flame impingement cases was intimately related to the location of the inner reaction zone with respect to the surface. Peak heat flux was obtained when the tip of the inner reaction zone just touched the impingement surface. There was a secondary peak in stagnation point heat flux (because of flow acceleration resulted from convergence of flow streamlines) when the target plate was some distance away from the tip of the reaction zone.
2. A reasonably accurate correlation fit for stagnation point Nusselt number was possible in the region (along axial length) between the tip of the inner reaction zone till the secondary rise in heat flux.
3. Simulation results showed that this high value of heat flux when the inner reaction zone just touched the impingement surface corresponded to high axial temperature gradient as well as high axial and radial velocity gradients.
4. For small H/d (= 3), the presence of the plate reduces the flame length compared to the free flame and very significantly alters the unburnt gas centerline velocity. For large ($H/d = 9$), the influence of the plate on the flame length and un-burnt gas centerline velocity is negligible.

5. For the 8-mm-diameter burner, detailed analysis of the simulation results indicate that for $H/d = 9$, the axial velocity gradient (at the plate) is higher and the temperature gradient is lower compared to $H/d = 5$ or 7. The combined effect of these is an almost constant stagnation point heat flux in the above H/d range. As indicated by the experimental results, there can even be a secondary peak in the stagnation point heat flux for low flow rates and larger burner diameters.

Acknowledgements

The first author is thankful to All India Council of Technical Education (AICTE) for sponsoring him for this research program. He is also thankful to National Institute of Technology, Jalandhar (Punjab) for granting him study leave for this research.

References

[1] C.E. Baukal, B. Gebhart, A review of flame impingement heat transfer studies Part 1: experimental conditions, Combust. Sci. Technol. 104 (1995) 339–357.
[2] M. Sibulkin, Heat transfer near the forward stagnation point of the body of revolution, J. Aero. Sci. 19 (1952) 570–571.
[3] J.K. Kilham, M.R.I. Purvis, Heat transfer from hydrocarbon – oxygen flames, Combust. Flame 16 (1971) 47–54.
[4] R. Conolly, R.M. Davies, A study of convective heat transfer from flames, Int. J. Heat Mass Transfer 15 (1972) 2155–2172.
[5] M. Fairweather, J.K. Kilham, A. Mohebi – Ashtiani, Stagnation point heat transfer from turbulent methane/air flames, Combust. Sci. Technol. 35 (1984) 225–238.
[6] M. Fairweather, J.K. Kilham, S. Nawaz, Stagnation point heat transfer from laminar high temperature methane/air flames, Int. J. Heat and Fluid Flow 5 (1) (1984) 21–27.
[7] G.K. Hargrave, M. Fairweather, J.K. Kilham, Forced convection heat transfer from impinging flames. Part II: Impingement heat transfer, Int. J. Heat and Fluid Flow 8 (1987) 132–138.
[8] T.H. van der Meer, Stagnation point heat transfer from turbulent low Reynolds number jets and flame jets, Experimental Thermal and Fluid Science 4 (1991) 115–126.
[9] L.L. Dong, C.S. Cheung, C.W. Leung, Heat transfer from an impinging pre-mixed butane/air slot flame jet, Int. J. Heat Mass Transfer 45 (2002) 979–992.
[10] L.L. Dong, C.S. Cheung, C.W. Leung, Heat transfer of an impinging butane/air flame jet of low Reynolds number, Experimental Heat Transfer 14 (2001) 265–282.
[11] L.L. Dong, C.S. Cheung, C.W. Leung, Heat transfer from an impinging pre-mixed butane/air slot flame jet, Int. J. Heat Mass Transfer 45 (2002) 979–992.
[12] L.C. Kwok, C.S. Cheung, C.W. Leung, Heat transfer characteristics of slot and round pre-mixed impinging butane/air flame jet, Experimental Heat Transfer 16 (2003) 111–137.
[13] A. Milson, N.A. Chigier, Studies of methane and methane/air flames impinging on cold plate, Combust. Flame 21 (1973) 295–305.
[14] J.R. Rigby, B.W. Webb, An experimental investigation of diffusion flame jet impinging heat transfer, Proc. ASME/JSME Therm. Eng. Conf. vol. 3 (1995) 117–126.
[15] S. Chander, A. Ray, Influence of burner geometry on heat transfer characteristics of methane/air flame impinging on flat surface, Exp. Heat Transfer 19 (1) (2006) 15–38.
[16] R. Viskanta, Heat transfer to impinging isothermal gas and flame jets, Exp. Therm. Fluid Sci. 6 (1993) 111–134.
[17] R. Viskanta, Convective and radiative flame jet impingement heat transfer, Int. J. Transport Phenom. 1 (1998) 1–15.
[18] S. Chander, A. Ray, Flame impingement heat transfer – a review, Energy Convers. Manage. 46 (18–19) (2005) 2803–2837.
[19] M.J. Remie, M.F.G. Cremers, K.R.A.M. Schreel, L.P.H. de Goey, Analysis of the heat transfer of an impinging laminar flame jet, Int. J. Heat Mass Transfer 50 (2007) 2816–2827.
[20] M.J. Remie, M.F.G. Cremers, K.R.A.M. Schreel, L.P.H. de Goey, Flame jet properties of Bunsen-type flames, Combust. Flame 147 (3) (2006) 163–170.
[21] C.R. Kleijn, Heat transfer from laminar impinging methane air flames, in: Proceedings of the 2001 ASME-PVP Conference 3rd Int. Symp. Comp. Techn. Fluid/Thermal/Chemical Systems Ind. Appl. Atlanta, Georgia, USA (2001) pp. 1–11 July 22–26.
[22] T. Poinsot, T. Echekki, M. Mungal, A study of the laminar flame tip and implications for premixed turbulent combustion, Combust. Sci. Technol. 81 (1992) 45–73.
[23] S. Chander, A. Ray, Heat transfer characteristics of three interacting flame jets impinging on flat surface, Int. J. Heat Mass Transfer 50 (3–4) (2007) 640–653.
[24] S.J. Kline, F.A. McClintock, Describing uncertainties in single sample experiments, Mech. Eng. 75 (1953) 3–8.
[25] S.G. Tuttle, B.W. Webb, M.Q. McQuay, Convective heat transfer from a partially premixed impinging flame jet. Part I: Time-averaged results, Int. J. Heat Mass Transfer 48 (7) (2005) 1236–1251.
[26] Fluent User Guide, vol. 1-4, FLUENT 6.1, 2003.
[27] C.J. Hoogendoorn, C.O. Popiel, T.H. van der Meer, Turbulent heat transfer on a plane surface in impinging round pre-mixed flame jets, in: Proc. of the 6th Int. Heat Trans. Conf., Toronto 4, 1978, pp. 107–112.
[28] R.A. Strehlow, Combustion Fundamentals, McGraw Hill Publication, New York, 1984, 344 Chapter 10.
[29] C.E. Baukal, B. Gebhart, Surface condition effect on flame impingement heat transfer, Experimental Thermal and Fluid Science 15 (1997) 323–335.